CRYSTAL GROWTH & DESIGN

pubs.acs.org/crystal

Article

Open Access

This article is licensed under CC-BY 4.0

Incommensurate Displacive and Occupational Modulation in Hexakis(Urea-*O*)Iron(III) Nitrate

Laura Bereczki, Kende Attila Béres, Eva Kovats, Attila Benyei, Robert Hühn, Džonatans Miks Melgalvis, Zoltan Homonnay, László Kótai, Petra Bombicz, and Toms Rekis*

Cite This: *Cryst. Growth Des.* 2025, 25, 1148−1154

Read Online

ACCESS | Metrics & More | Article Recommendations

ABSTRACT: The structure of hexakis(urea-*O*)iron(III) nitrate is found to be incommensurately modulated. It is described in (3 + 1)-dimensional superspace adopting the superspace group $C2/c(\sigma_1 0 \sigma_3)00$ with the modulation wavevector $\mathbf{q} = -0.7394(7)\mathbf{a}^* + 0.9390(8)\mathbf{c}^*$. Up to the third-order satellite reflections are observed in the diffraction data collected at 100 K. Consequently, there is an anharmonic displacive modulation present in the hexacoordinated iron(III) complex. Nitrate ions are found in two symmetrically independent sites in the unit cell and form two disordered ensembles with three disordered components and two disordered components, respectively. The latter site is located near a 2-fold axis, resulting in a total of four disorder components for this molecular site. Along with the displacive modulation for the nitrate ions, there is also a complex occupational modulation present. Possible origins of the modulation are discussed.

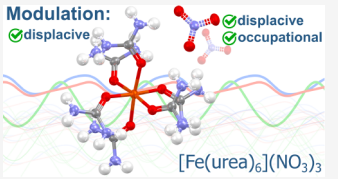

Downloaded via 31.46.112.87 on March 7, 2025 at 17:56:49 (UTC).
See https://pubs.acs.org/sharingguidelines for options on how to legitimately share published articles.

INTRODUCTION

Modulated crystal structures have long been known to exist[1] and the formal description of such structures within the superspace framework is well established.[2,3] Nevertheless, the occurrence of modulated phases is rare and sometimes ignored.

Unlike ordinary crystal structures, incommensurately modulated phases lack 3-dimensional translational symmetry. This symmetry is, however, present in a higher-dimensional space. For example, for a (3 + 1)-dimensional structure, there is an additional dimension $\overline{x}_4 \in [0, 1)$ present. The structure is described in a 3-dimensional unit cell with atomic positions $\mathbf{x}^0$ (basic positions) and modulation functions $\mathbf{u}(\overline{x}_4)$. The basic position of an atom has little physical meaning since the real position with respect to the unit cell is obtained by adding the modulation function values to the basic position coordinates at a specific argument value $\overline{x}_4$ in superspace: $\mathbf{x} = \mathbf{L} + \mathbf{x}^0 + \mathbf{u}(\overline{x}_4)$, where $\mathbf{L}$ are lattice vectors of the basic structure, $\mathbf{u}$ is the periodic modulation function with the argument $\overline{x}_4 = t + \mathbf{q}\cdot(\mathbf{L} + \mathbf{x}^0)$, which includes the modulation period t and the dot product of the modulation wavevector $\mathbf{q}$ and the basic position $\mathbf{L} + \mathbf{x}^0$. The actual structure model can be created by setting $t = 0$ and calculating the atomic positions from $\mathbf{x}^0$ and $\mathbf{u}$ for the unit cell $\mathbf{L} = (0, 0, 0)$ and advancing $\mathbf{L}$ in each of the three spatial directions. In addition, unit cell symmetry is taken into account. Such a structure description is not practical since the components of $\mathbf{L}$ are not bounded. Furthermore, a different t value can be chosen for the structure model construction starting from the "origin" unit cell $\mathbf{L} = (0, 0, 0)$. This demonstrates the very essence of the lack of 3-dimensional translation symmetry in incommensurately modulated phases.

Because the translational periodicity is present in superspace, it is practical to describe the structure using so-called *t*-plots. In such a plot, all occurring values of a certain parameter are summarized in a manner that encompasses the long-range order in a modulated crystal structure. For example, by plotting $x_y = x_y^0 + u_y(t + \mathbf{q}\cdot\mathbf{x}^0)$ versus t of a certain atom will summarize all possible (infinitely many) fractional y coordinates found in the crystal structure for the atom in question. In addition to the description of the displacive modulation of the atoms, all occurring distances or angles between two chosen atoms or any other geometrical parameters derived from the atomic positions, such as torsion angles, can be summarized in *t*-plots. Furthermore, modulation function parameters for atomic displacement parameters can be refined if the data allow it. Finally, an occupational modulation can be present, meaning that at different t values, the occupation of an atom differs. Summarizing such an incommensurately modulated structure in *t*-plots allows us to represent it in a concise manner and analyze the crystal chemistry.

We report here a (3 + 1)-dimensional structure of hexakis(urea-*O*)iron(III) nitrate that was found to be

Received: October 22, 2024
Revised: January 28, 2025
Accepted: January 29, 2025
Published: February 4, 2025

© 2025 The Authors. Published by American Chemical Society

incommensurately modulated, displaying displacive and complex occupational modulation. This compound is extensively studied, for example, for obtaining magnetic nanopowders.[4−6] Nevertheless, the structure has not been previously published despite some attempts to determine it.[7]

EXPERIMENTAL SECTION

Synthesis and Growth of Single Crystals. Synthesis of hexakis(urea-*O*)iron(III) nitrate was done as described in the literature.[8] An 8.08 g (0.02 mol) of iron(III) nitrate nonahydrate and a 7.21 g (0.12 mol) of urea were mixed together in a 25 mL beaker and dissolved in 9.50 mL of distilled water. The resulting orange solution was left to evaporate. After 2 days, the compound had crystallized in a few millimeters of large light blue crystals. The formed crystals were filtrated off on a G2 glass filter and washed with cold (0°C) distilled water, absolute ethanol, and diethyl ether, respectively, and left to dry in a desiccator containing P_2O_5 for 12 h. The yield was 93%. The crystals were cut, and a crystal with a size of (0.14 × 0.10 × 0.06) mm^3 was chosen for X-ray diffraction measurements.

Mössbauer Spectroscopy Measurements. The measurements were carried out on a WissEl type spectrometer, in the speed range of 12 mm s^{-1}, operating in constant acceleration mode and at liquid nitrogen temperature. The radiation source was ^{57}Co in a Rh matrix with an activity of 0.74 GBq. The samples were kept in an SVT-400-MOSS cryostat. The isomer shift is given relative to that of α-iron. The Mössbauer spectra were evaluated using MossWinn software[9] that provide standard computer-based statistical analysis methods. This included fitting the experimental data by a sum of Lorentzians or relaxation line shapes using a least-squares minimization procedure.

Collection of the Diffraction Data. The data were collected at the PETRA III synchrotron facility at the DESY in Hamburg, Germany. A Huber 4-circle diffractometer equipped with a Lambda detector from X-Spectrum (CdTe, pixel size: (0.055 × 0.055 mm^2) was used at the Experimental Hutch EH2 at beamline P24. The synchrotron radiation was set to a wavelength of λ = 0.500016 Å and operated in a 40-bunch mode. ϕ-Scans were performed in the range of 0°−360° with 0.1° steps and an exposure time of 0.4 s. The single-crystal sample was maintained at a temperature of 100 K using a nitrogen gas jet cryostat.

Diffraction Data Integration and Structure Solution. The diffraction data of the title compound $[Fe(CO(NH_2)_2)_6](NO_3)_3$ show a *C*-centered monoclinic lattice with satellite reflections. Up to the third-order satellite reflections ($0 < |m| \leq 3$) can be observed in the reciprocal space reconstruction layers (see Figure 1). The modulation wavevector can be chosen and refined as $\mathbf{q} = [-0.7394(7), 0, 0.9390(8)]$, which is consistent with a decreasing average intensity of the satellite reflections with increasing $|m|$. Furthermore, $\mathbf{q}$ is consistent with the monoclinic symmetry.

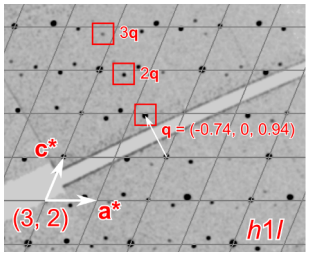

Figure 1. Reconstruction of the *h1l* reciprocal layer showing a *C*-centered lattice and satellite reflections.

Data were integrated using CrysAlisPro version 1.171.41.115a software. The *C*-centered lattice setting was used, and Laue class *2/m* was applied for outlier detection. The data were imported into JANA2006 software[10] and averaged. The R_{int} values are listed in Table 1.

Table 1. Statistics on Reflection Averaging

	Satellite index	0 (main)	±1	±2	±3
Obs.	R_{int}/ %	4.58	6.40	11.51	23.32
	Number	2939	5723	4379	1545
	Averaged from	16287	31825	25288	9315
All	R_{int}/ %	4.88	7.42	16.69	67.91
	Number	4514	9006	9003	8943
	Averaged from	25177	50290	51210	51460

The structure solution was performed with the SUPERFLIP software.[11]

Structure Refinement. The structure was refined using the JANA2006 software suite.[10] Initially, the iron atom and ligands were located, and their basic positions were refined based on the main reflections. Furthermore, refinement in the superspace was advanced. For the iron atom, positional and anisotropic atomic displacement parameters (ADPs) were refined together with modulation function coefficients for displacive modulation and modulated atomic displacement (up to third-order harmonics).

There are three urea ligands in the asymmetric unit for which the rigid-body model was used. The basic positions and ADPs of all four non-hydrogen atoms of the urea molecule were refined freely. A riding model was used for the hydrogen atoms. Translational and rotational parameters for the two additional positions of urea molecules were refined. Parameters for a displacive modulation (up to third-order harmonics) were refined for all three urea molecules. TLS parameters were refined to model the thermal displacement of the rigid body in superspace (first-order harmonics).

Nitrate ions were treated as rigid bodies, and their treatment was similar to that of urea molecules, i.e., the displacive modulation was refined using up to the third-order harmonics. Up to the third-order harmonics were also used for the occupational modulation.

Relevant crystallographic parameters are summarized in Table 2.

Models with Alternative Symmetry and Possible Twinning. We have considered alternative superspace groups and possible twinning. There are two superspace groups based on the basic symmetry *C2/c*, namely $C2/c(\sigma_1 0 \sigma_3)00$ (used in this study) and $C2/c(\sigma_1 0 \sigma_3)0s$. The latter superspace group was not considered because 1930 satellite reflections (including 391 observed reflections) violated this superspace group symmetry, with the strongest absent reflections having an $I/\sigma(I) > 20$.

The absence of inversion symmetry was considered. The superspace group $Cc(\sigma_1 0 \sigma_3)0$ led to a satisfactory refinement but with *R* values slightly higher than for the monoclinic model presented in the study. This means that the presented model fits better to the data than does this *Cc* model (with around 200 more parameters to refine). Furthermore, the superspace

https://doi.org/10.1021/acs.cgd.4c01457
Cryst. Growth Des. 2025, 25, 1148−1154

Table 2. Crystallographic Data of the Hexakis(Urea-O)Iron(III) Nitrate Structure in (3 + 1)-Dimensional Superspace

Formula	$Fe_{0.5}\ C_3\ H_{12}\ N_{7.5}\ O_{7.5}$
Formula (refined)	$Fe_{0.5}\ C_3\ H_{12}\ N_{7.458}\ O_{7.373}$
Formula weight/g mol-*1*	298.47
t/K	100
Crystal system	monoclinic
Superspace group	$C2/c(\sigma_1 0\sigma_3)00$
q	$-0.7394(7)\mathbf{a}^* + 0.9390(8)\mathbf{c}^*$
a/ Å	11.1534(4)
b/ Å	18.6443(6)
C/ Å	12.1716(5)
β/ °	112.380(4)
V/ Å^3	2340.40(15)
Z, *Z*′	4, 0.5
F(000)	1233
D_x/ g cm^{-3}	1.6942
μ/ mm^{-1}	0.279
λ/ Å	0.500016
Measured reflections	178137
Unique reflections	31466
Observed reflections	14586
Refinement method	Full-matrix least-squares on *F*
No. of parameters	600
R_1 (obs.)	0.0887
R_1 (obs., $m = 0$)	0.0762
R_1 (obs., $m = \pm1$)	0.0833
R_1 (obs., $m = \pm2$)	0.0998
R_1 (obs., $m = \pm3$)	0.1840
wR (all)	0.1103
wR (all, $m = 0$)	0.1086
wR (all, $m = \pm1$)	0.1033
wR (all, $m = \pm2$)	0.1091
wR (all, $m = \pm3$)	0.2424
GoF (all)	3.08
H-atom treatment	riding model
Weighting scheme	$w = 1/(\sigma^2(F) + 0.0001F^2)$
Δ_{max}/ Å^{-3}	1.85
Δ_{min}/ Å^{-3}	−1.32
Condition for obs. rflns.	$I > 3\sigma(I)$

group $C2(\sigma_1 0\sigma_3)0$ was considered, but refinement did not converge well and led to distorted geometry and unrealistic atomic displacement parameters.

Finally, pseudomerohedral twinning was considered, which is commonly observed for modulated structures. The highest metric symmetry is monoclinic in this case, and only triclinic superspace groups must be considered. We did not find any peak splitting in the data, indicating a deviation from monoclinic symmetry. This is, of course, not the definitive proof for the lack of pseudomerohedral twinning since the deviation of the metric symmetry can be infinitely small. Alternatively, only a single twin domain could have been present, i.e., the structure is triclinic with no twinning.

Therefore, we considered the structure to be triclinic and performed a refinement in the superspace group $C\ -1-(\sigma_1\sigma_2\sigma_3)0$, but the *R* values were a few percentage points higher than those of the best monoclinic model. Additionally, the refined twin volume for the second domain was 0.498, which is close to 0.5 and means that either the twin domain fraction is indeed 1:1 or the data represent a monoclinic structure.

RESULTS AND DISCUSSION

Insights from the Mössbauer Spectroscopy Studies. Elucidating the structural model of the studied compound is challenging for several reasons. Both molecular entities, namely, urea and nitrate ions have similar shapes and are composed of atoms with similar scattering power. Iron is known to coordinate with both urea molecules and nitrate ions.[12−14] Both ligands are considered weak field ligands, and the resulting octahedral iron(III) high-spin complexes would be substitutionally labile. Furthermore, the structure is modulated, and preliminary studies revealed the presence of substantial disorder. Finally, the compound was crystallized from an aqueous solution, meaning that water molecules could potentially be included in the structure. To guide the structure elucidation, valuable information was obtained through Mössbauer spectroscopy studies.

The Mössbauer spectra of the studied compound were recorded at 90 K (see Figure 2). The spectra are similar to the previously studied hexakis(urea-*O*)iron(III) complexes.[15−19] It contains one broadened Lorentzian singlet with a line width of 0.63 mm s^{-1}. Based on the isomer shift *δ*, the sample exhibits only one high-spin iron(III) complex chemical environment. There is no quadrupole splitting present; therefore, the ligand field is symmetric around the central Fe^{3+} ion. These results indicate that the iron atom is indeed coordinated by six urea ligands, and for the charge balance, three nitrate ions per one iron atom are present in the structure.

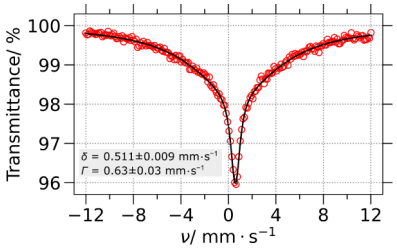

Figure 2. Mössbauer spectra of the studied complex were recorded at 90 K.

Displacive Modulation of the Iron−Urea Complex Moiety. The irrational components of the modulation wavevector **q** and the strong second-order satellite reflections visible in the diffraction data indicate an anharmonic incommensurate modulation present in the structure of the title compound. Indeed, the iron atom is displaced from its basic position in the unit cell anharmonically, as can be seen in Figure 3.

The iron atom is found on the 2-fold axis (2_y) which induces constraints on the modulation function parameters. The resulting symmetry of the displacive modulation in superspace can be best noted in the x_4-plot in Figure 3. The modulation function $u_y(\bar{x}_4)$ is therefore even, but modulation functions $u_x(\bar{x}_4)$ and $u_z(\bar{x}_4)$ are odd (note that $\bar{x}_4 = t + \mathbf{q}\cdot\mathbf{x}^0$). For the iron atom, the largest displacement range of around 0.8 Å occurs along the unique axis (*b*) of the monoclinic unit cell. The displacement range along the *a*- and *c*-axes is approximately 0.4 Å.

https://doi.org/10.1021/acs.cgd.4c01457
Cryst. Growth Des. 2025, 25, 1148−1154

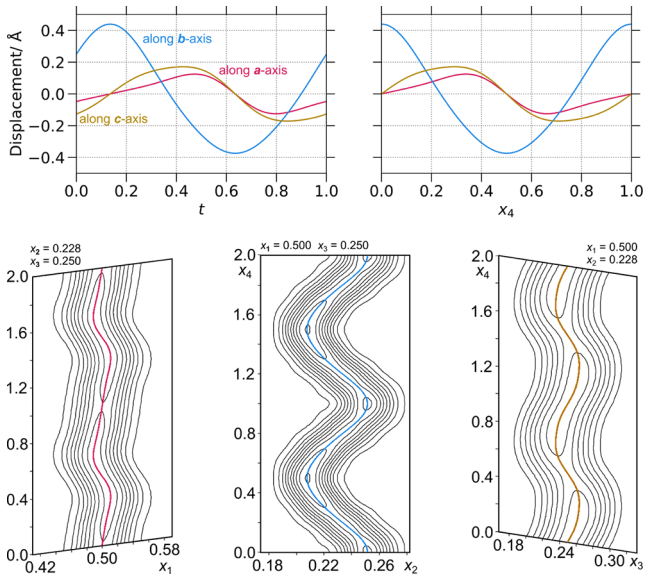

Figure 3. Displacive modulation of the Fe atom. Top: *t*- and x_4-plots of the Fe atom displacement along each unit cell axis. Bottom: de Wolff's sections of the Fe atom showing the electron density contours based on F_{obs} and calculated in a 2 Å scope.

The iron in the studied complex is octahedrally coordinated by six urea ligands. The coordination occurs through the oxygen atoms, which is typical also for other hexakis(urea-*O*)-iron salts.[20] There are three urea molecules in the asymmetric unit, while the rest are related by 2-fold symmetry (see Figure 4).

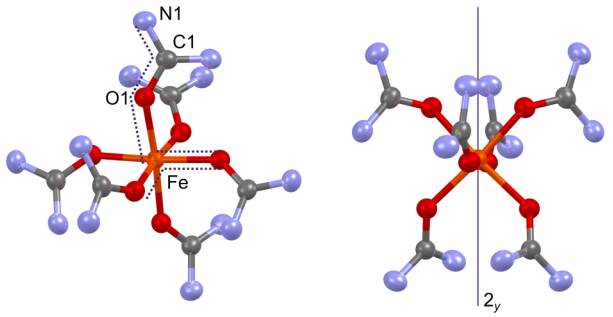

Figure 4. Basic structure of the $[Fe(CO(NH_2)_2)_6]^{3+}$ complex (hydrogen atoms are omitted for clarity). Left: the octahedral geometry is shown indicating parameters that are explored along the additional dimension in the superspace (Fe−O distances, O−Fe−O angles, and Fe−O−C−N torsion angles). Right: the 2-fold (2_y) symmetry of the complex is shown.

The geometry of the complex moiety was explored along the additional dimensions in the superspace. Specifically, the Fe−O distances, the O−Fe−O angles, and the Fe−O−C−N torsion angles were explored. The Fe−O distances of the three symmetrically independent fragments were found to be very rigid (see Figure 5 top left). The distances do not deviate considerably from around 2.0 Å. Indeed, the structure must be chemically and physically plausible. A survey in the Cambridge Structural Database (v 5.45[21] indicates that Fe^{3+}−O distances in octahedrally coordinated nonmodulated complexes show a narrow distribution centered around 2.0 Å (Figure 5 top right), which means that such coordination bond is not affected by the crystal field. This fact means that also in modulated structures, the particular distance should not display any notable variation along additional dimensions in superspace. The survey in the database corroborates that iron is indeed in its +3 oxidation state in the studied complex. Note that a separate distribution centered at 2.1 Å is present for other iron complexes. For those, the oxidation state of iron is reported to be +2.

As far as the studied structure is concerned, the urea ligands are modulated completely with the already described displacive modulation of the iron atom. Furthermore, the octahedral geometry is also rigid along the additional dimensions in the superspace. The O−Fe−O angles are approximately 90° along the modulation period *t* (see Figure 5 bottom left). Notable modulation, however, is present for the torsion angles associated with the orientation of the urea ligands with respect to the coordination octahedra. The particular torsion angles are modulated in a range from around 10−25° (see Figure 5 bottom right). This observation is consistent with similar iron−urea complexes, where the particular torsion angles are found to be in the range of 10−40°. The orientation of the urea ligands is apparently easily influenced by the crystal field, as there is no constant value found for other (nonmodulated) iron-urea complexes. In the studied modulated structure, the chemical environment depends on the modulation period *t*, which results in the respective torsion angle variation.

Displacive and Occupational Modulation of the Nitrate Anions. The Mössbauer spectroscopy data indirectly indicated that 1.5 nitrate ions must be present in the asymmetric unit to ensure the charge balance. Nitrate ions were found in two sites in the unit cell. In site 1, there are three disorder components present (*a*, *b*, and *c*). This site should account for one full nitrate ion. The remaining half a nitrate ion in the asymmetric unit is a crystallographic formality since molecules exist as individual discrete entities. The symmetry of the nitrate ion is compatible with the 2-fold axis present in the unit cell. However, no nitrate ion was found on the 2-fold axis. Instead, two nitrate ions were found in the close vicinity of the 2-fold axis with all atoms at general positions. This leads to the second disorder ensemble (site 2) with two symmetrically independent disorder components. Taking into account the 2-fold axis, this results in four disorder components for the molecular site in question (see Figure 6).

Initially, crenel functions were considered for refinement because each disorder component was found at a different *t* interval, and no clear overlap of two or more disorder components at a specific *t* value could be observed. In such a model, in its simplest form, all disorder components with full occupancy would be found at different *t* intervals so that individual intervals do not overlap but cover the full modulation period. However, such refinement did not give satisfactory results. Instead, occupational modulation was considered with occupation modulation function maxima centered at *t* values, where each individual nitrate ion was most clearly visible in the Fourier difference maps. The refinement converged, resulting in a chemically sensible structure model.

In Figure 7, *t*-plots of the occupational modulation of the nitrate ion disorder components are shown for sites 1 and 2. The occupational modulation was refined without any constraints. Yet, it resulted in a chemically sensible model for sites 1 and 2. For site 1, the sum of all three modulation functions should not exceed 1.0 at any given *t*. Unless a vacancy is considered, the sum of the three occupational

https://doi.org/10.1021/acs.cgd.4c01457
Cryst. Growth Des. 2025, 25, 1148−1154

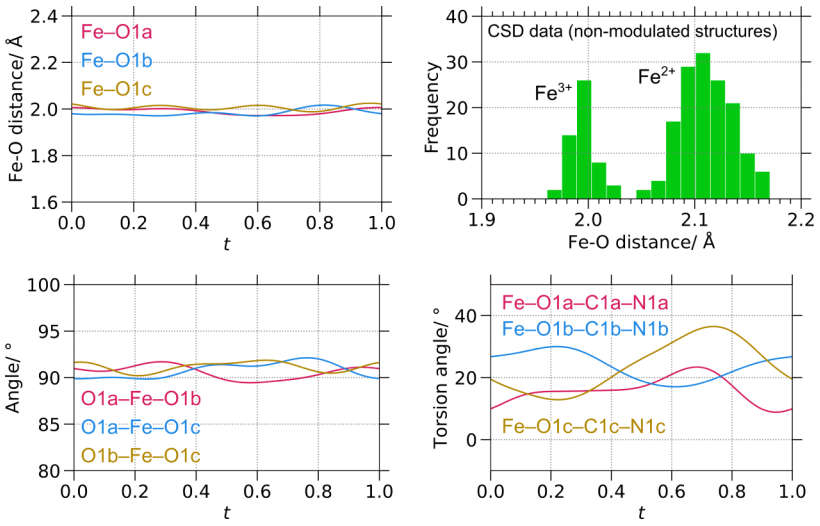

Figure 5. *t*-Plots showing modulation of the $[Fe(CO(NH_2)_2)_6]^{3+}$ complex geometric parameters and distribution of Fe−O distances in similar octahedrally coordinated iron compounds with oxygen-containing ligands.

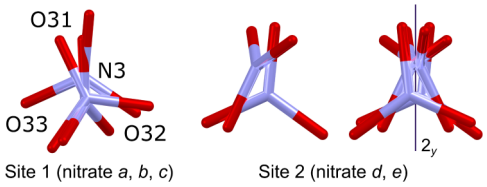

Figure 6. Representation of the nitrate ion disorder ensembles, as found in the basic structure. The atoms of the nitrate ions are numbered as follows: N3, O31, O32, and O33 with added letters *a*, *b*, *c*, *d*, or *e* to specify the actual disorder component.

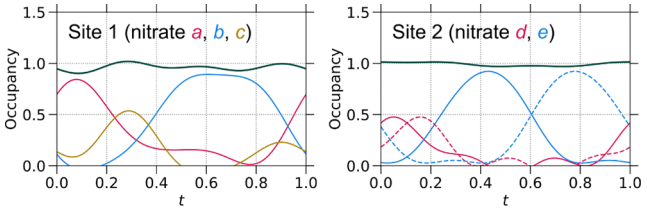

Figure 7. *t*-Plots showing the occupational modulation of the nitrate ion disorder components in sites 1 and 2. For site 2, occupancy functions of the symmetry-related $(-x + 1, y, -z - 1/2)$ nitrate ions are given. The green curves are sums of the depicted occupancy modulation functions.

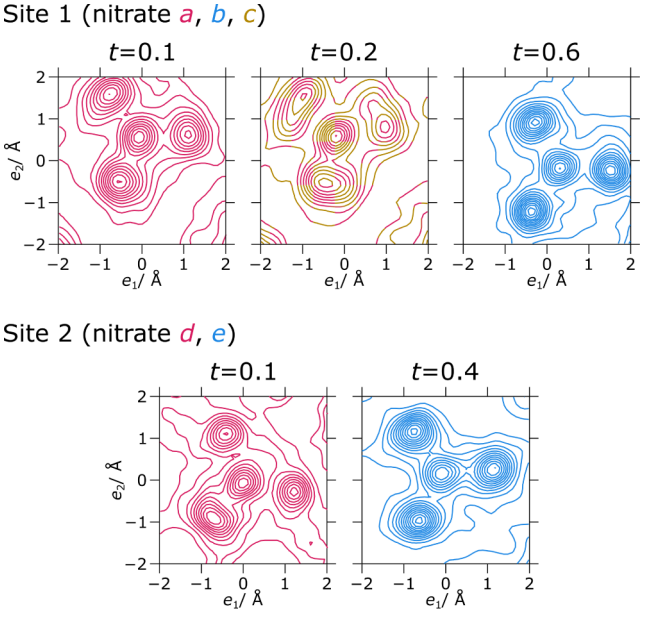

Figure 8. Electron density map projections (summed along e_3) calculated based on F_{obs} in a 4 × 4 × 4 angstrom scope for selected *t* values. The density maps are centered at the basic position of the N3 atom of each nitrate entity with atoms N3, O31, and O32 being in the plane e_1e_2.

modulation functions should be 1.0, indicating that there is one full nitrate anion in site 1 throughout the crystal structure. As can be seen in Figure 7, the sum for site 1 is indeed close to 1.0 at any given *t*.

For site 2, the 2-fold axis needs to be taken into account. In the *t*-plot in Figure 7, the modulation functions for both disorder components *d* and *e* are depicted together with the symmetry-related nitrate moieties (symmetry code: $-x + 1$, *y*, $-z - 1/2$). The sum of all four modulation functions is very close to 1.0 at each *t*, even though no constraints were used. These results show that despite the complex disorder and no constraints used for the occupancy refinement in superspace, a correct charge balance is reached for the structure model. Further evidence for validity is given in Figure 8 where electron density maps at selected *t* values for nitrate sites 1 and 2 are depicted.

For site 1 at around $t = 0.1$, disorder component *a* has the largest occupancy. This is clearly visible in the density map projection. At $t = 0.2$, disorder components *a* and *c* have occupancies of 0.58 and 0.38, respectively. Both disorder components lie in approximately the same plane. Taking into account the additional displacive modulation at $t = 0.2$, atoms N3a and N3c are nearly overlapping, while the oxygen atoms in pairs of O31a/O31c, O32a/O32c, and O33a/O33c are all shifted by around 0.9 Å. The splitting of the oxygen atom positions is clearly visible in the density map. The occupancy of disorder component *b* at $t = 0.2$ is close to 0.0, and it is therefore not visible in the density map projections. At $t = 0.6$, however, the occupancy of disorder component *b* reaches its maximum, and this is clearly visible in the electron density map.

https://doi.org/10.1021/acs.cgd.4c01457
Cryst. Growth Des. 2025, 25, 1148−1154

For site 2, disorder components *d* and *e* are also visible in the density maps in Figure 8. Component *d* is best visible at t = 0.1, where its occupancy is 0.43. Component *e* is clearly visible at t = 0.4, where its occupancy is 0.91.

General Organization of the Structure. The structure of hexakis(urea-*O*)iron(III) nitrate can be regarded as a monoclinic distortion of a higher symmetry trigonal structure. Such monoclinic distortions of trigonal symmetry structures are known.[22,23] In Figure 9 left, the packing representation of

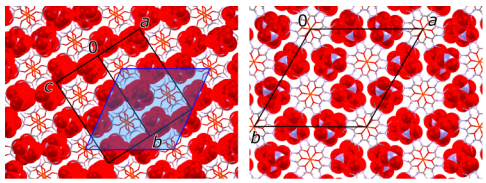

Figure 9. Packing representation of the basic structure of the studied complex with a putative distorted trigonal unit cell shaded in blue (left), the nonmodulated structure of a related compound $[Fe(1,1\text{-dimethylurea})_6](NO_3)_3$ hydrate. Iron complex moieties are represented with rods, and nitrate ions are represented with spheres.

the basic structure of the studied compound is shown along $(\vec{a} + \vec{c})$-direction. A honeycomb pattern can be observed where columns of $[Fe(CO(NH_2)_2)_6]^{3+}$ complex moieties are surrounded by 6 columns of nitrate ions. Similar structural organization is observed in a related compound $[Fe(1,1\text{-dimethylurea})_6](NO_3)_3$ hydrate[24] in $R\bar{3}R\bar{3}$ (see Figure 9 right).

We further discuss possible origins of the modulation related to hydrogen bonding. First of all, hydrogen bonding can be identified between the oxygen atoms of the urea ligands and the hydrogen atoms of the neighboring ligand urea molecules (see Figure 10 left).

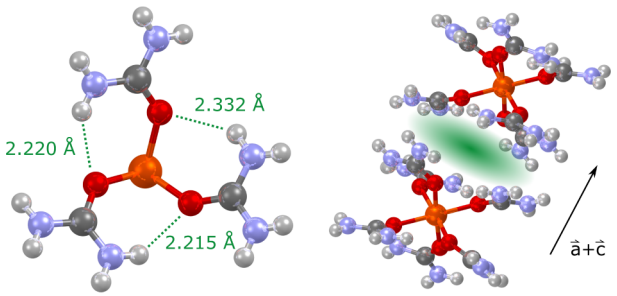

Figure 10. Left: asymmetric unit of the complex moiety showing hydrogen bonding in the basic structure. Right: two neighboring complex moieties sharing faces of six amino groups, between which hydrogen bonding is possible.

Second of all, two neighboring complex moieties are sharing faces rich in hydrogen bond donors and acceptors (see Figure 10 right) between which hydrogen bonding of different strengths is possible. Note that we do not analyze the exact geometrical parameters of hydrogen bonding entities (D−H···A) along the additional dimension in superspace since the positions of the hydrogen atoms were not refined but added geometrically. There is a crucial degree of freedom present, i.e., the rotation along each of the six asymmetric $C-NH_2$ bonds that were not refined. We suspect that the modulation observed in this structure is related to the optimization of the hydrogen bonding network along the $[Fe(CO(NH_2)_2)_6]^{3+}$ moiety columns. Furthermore, we argue that the complex occupational and displacive modulation of the nitrate ions is related to the hydrogen bonding between the nitrate ions and the neighboring amino groups of the urea ligands found in the neighboring columns.

CONCLUSIONS

The structure of hexakis(urea-*O*)iron(III) nitrate displays an anharmonic displacive modulation of the $[Fe(CO(NH_2)_2)_6]^{3+}$ complex entities, which is accompanied by displacive and occupational modulation of the nitrate anions. The overall organization of the monoclinic structure can be regarded as a trigonal distortion with columns of the complex moieties and columns of nitrate ions. It is suspected that the modulation, especially the occupational modulation of the nitrate ions, is present to optimize the hydrogen bonding network in the channels with extensive hydrogen bond donors (amino groups of the urea ligands) present. We found that additional information gained from an additional method (Mössbauer spectroscopy in this case) can be very useful to aid model refinement of such a complex modulated structure.

ASSOCIATED CONTENT

Accession Codes

Deposition Number 2392180 contains the supplementary crystallographic data for this paper. These data can be obtained free of charge via the joint Cambridge Crystallographic Data Centre (CCDC) and Fachinformationszentrum Karlsruhe Access Structures service.

AUTHOR INFORMATION

Corresponding Author

Toms Rekis − *Institute for Inorganic and Analytical Chemistry, Goethe-University Frankfurt, Frankfurt am Main 60438, Germany; Faculty of Medicine and Life Sciences, University of Latvia, Riga LV1004, Latvia;* orcid.org/0000-0001-5128-4611; Email: rekis@chemie.uni-frankfurt.de

Authors

Laura Bereczki − *Institute of Materials and Environmental Chemistry and Centre for Structural Science, HUN-REN Research Centre for Natural Sciences, Budapest 1117, Hungary;* orcid.org/0000-0003-0615-4361

Kende Attila Béres − *Institute of Materials and Environmental Chemistry, HUN-REN Research Centre for Natural Sciences, Budapest 1117, Hungary; György Hevesy PhD School of Chemistry, Institute of Chemistry, Eötvös Loránd University, Budapest 1117, Hungary;* orcid.org/0000-0003-4257-0581

Eva Kovats − *Institute for Solid State Physics and Optics, Wigner Research Centre for Physics, Budapest 1121, Hungary;* orcid.org/0000-0002-8358-857X

Attila Benyei − *Department of Physical Chemistry, University of Debrecen, Debrecen 4032, Hungary;* orcid.org/0000-0002-0617-6264

Robert Hühn − *Institute for Inorganic and Analytical Chemistry, Goethe-University Frankfurt, Frankfurt am Main 60438, Germany*

Džonatans Miks Melgalvis − *Faculty of Medicine and Life Sciences, University of Latvia, Riga LV1004, Latvia*

Zoltan Homonnay − *Institute of Materials and Environmental Chemistry, HUN-REN Research Centre for Natural Sciences, Budapest 1117, Hungary; György Hevesy PhD School of*

https://doi.org/10.1021/acs.cgd.4c01457
Cryst. Growth Des. 2025, 25, 1148−1154

Chemistry, Institute of Chemistry, Eötvös Loránd University, Budapest 1117, Hungary

László Kótai − *Institute of Materials and Environmental Chemistry, HUN-REN Research Centre for Natural Sciences, Budapest 1117, Hungary*

Petra Bombicz − *Centre for Structural Science, HUN-REN Research Centre for Natural Sciences, Budapest 1117, Hungary;* orcid.org/0000-0002-5509-1515

Complete contact information is available at: https://pubs.acs.org/10.1021/acs.cgd.4c01457

Notes

The authors declare no competing financial interest.

■ ACKNOWLEDGMENTS

We acknowledge DESY (Hamburg, Germany), a member of the Helmholtz Association HGF, for the provision of experimental facilities. Parts of this research were carried out at PETRA III, and we would like to thank Martin Tolkiehn, Leila Noohinejad, and Preeti Pokhriyal for assistance in using the diffraction facility in the EH2 in beamline P24. Beamtime was allocated for proposal I-20221349 EC and R-20240678.

■ REFERENCES

(1) Janner, A.; Janssen, T. Symmetry of periodically distorted crystals. *Phys. Rev. B* **1977**, *15*, 643−658.

(2) van Smaalen, S. *Incommensurate Crystallography*; OUP Oxford, 2007.

(3) Janssen, T.; Chapuis, G.; de Boissieu, M. *Aperiodic Crystals: From Modulated Phases to Quasicrystals*; OUP Oxford, 2007.

(4) Carp, O.; Patron, L.; Diamandescu, L.; Reller, A. Thermal decomposition study of the coordination compound [Fe(urea)6]-(NO3)3. *Thermochim. Acta* **2002**, *390*, 169−177.

(5) Zhao, S.; Wu, H. Y.; Song, L.; Tegus, O.; Asuha, S. Preparation of γ-Fe2O3 nanopowders by direct thermal decomposition of Fe-urea complex: Reaction mechanism and magnetic properties. *J. Mater. Sci.* **2009**, *44*, 926−930.

(6) Asuha, S.; Zhao, S.; Wu, H.; Song, L.; Tegus, O. One step synthesis of maghemite nanoparticles by direct thermal decomposition of Fe−urea complex and their properties. *J. Alloys Compd.* **2009**, *472*, L23−L25.

(7) Durski, Z.; Gibiński, T. Determination of Space Groups and Lattice Constants of Crystals of $Cr(NO_3)3*6CO(NH_2)_2$ and $Fe(NO_3)3*6CO(NH_2)_2$. *Rocz. Chem.* **1972**, *46*, 1945−1952.

(8) Barbieri, G. A. Sui composti di ferriurea. *Rend. Atti Real. Accad Rend. Lincei.* **1913**, *22*, 867−870.

(9) Klencsár, Z.; Kuzmann, E.; Vértes, A. User-friendly software for Mössbauer spectrum analysis. *J. Radioanal. Nucl. Chem.* **1996**, *210*, 105−118.

(10) Petříček, V.; Dušek, M.; Palatinus, L. Crystallographic Computing System JANA2006: General features. *Z. Kristallogr. -Cryst. Mater.* **2014**, *229*, 345−352.

(11) Palatinus, L.; Chapuis, G. SUPERFLIP− a computer program for the solution of crystal structures by charge flipping in arbitrary dimensions. *J. Appl. Crystallogr.* **2007**, *40*, 786−790.

(12) Skodje, K. M.; Williard, P. G.; Kim, E. Conversion of Fe(NO)210 dinitrosyl iron to nitrato iron(iii) species by molecular oxygen. *Dalton Trans.* **2012**, *41*, 7849−7851.

(13) Wyllie, G. R. A.; Munro, O. Q.; Schulz, C. E.; Scheidt, W. R. Structural and physical characterization of (nitrato)iron(III) porphyrinates [Fe(por)(NO3)] − Variable coordination of nitrate. *Polyhedron* **2007**, *26*, 4664−4672.

(14) Kurtikyan, T. S.; Gulyan, G. M.; Minasyan, H. S.; Hovhannisyan, A. A.; Ford, P. C. Six-Coordinate Nitrato Complexes of Iron Porphyrins with Trans S-Donor Ligands. *Inorg. Chem.* **2018**, *57*, 4795−4798.

(15) Russo, U.; Calogero, S.; Burriesci, N.; Petrera, M. Mössbauer characterization of some new high-spin iron complexes with urea and thiourea derivatives. *J. Inorg. Nucl. Chem.* **1979**, *41*, 25−30.

(16) Galeazzi, G.; Russo, U.; Valle, G.; Calogero, S. Mössbauer study of some iron(III) complexes with urea type ligands and the crystal structure of hexakisdimethylureairon(III) perchlorate. *Transition Met. Chem.* **1981**, *6*, 325−328.

(17) Yamauchi, S.; Sakai, Y.; Tominaga, T. Paramagnetic relaxation effects on Mössbauer spectra of hexakis/alkylurea/iron/III/ complexes. *J. Radioanal. Nucl. Chem.* **1987**, *119*, 283−289.

(18) Béres, K. A.; Homonnay, Z.; Kvitek, L.; Dürvanger, Z.; Kubikova, M.; Harmat, V.; Szilágyi, F.; Czégény, Z.; Németh, P.; Bereczki, L.; Petruševski, V. M.; Pápai, M.; Farkas, A.; Kótai, L. Thermally Induced Solid-Phase Quasi-Intramolecular Redox Reactions of [Hexakis(urea-O)iron(III)] Permanganate: An Easy Reaction Route to Prepare Potential (Fe,Mn)Ox Catalysts for CO2 Hydrogenation. *Inorg. Chem.* **2022**, *61*, 14403−14418.

(19) Béres, K. A.; Homonnay, Z.; Barta Holló, B.; Gracheva, M.; Petruševski, V. M.; Farkas, A.; Dürvanger, Z.; Kótai, L. Synthesis, structure, and Mössbauer spectroscopic studies on the heat-induced solid-phase redox reactions of hexakis(urea-O)iron(III) peroxodisulfate. *J. Mater. Res.* **2023**, *38*, 1102−1118.

(20) Béres, K. A.; Homonnay, Z.; Kótai, L. Hexakis(urea-O)iron Complex Salts as a Versatile Material Family: Overview of Their Properties and Applications. *ACS Omega* **2024**, *9*, 11148−11167.

(21) Groom, C. R.; Bruno, I. J.; Lightfoot, M. P.; Ward, S. C. The Cambridge Structural Database. *Acta Crystallogr., Sect. B* **2016**, *72*, 171−179.

(22) Przeniosło, R.; Fabrykiewicz, P.; Sosnowska, I. Monoclinic deformation of calcite crystals at ambient conditions. *Phys. B* **2016**, *496*, 49−56.

(23) Bader, V. P.; Langmann, J.; Gegenwart, P.; Tsirlin, A. A. Deformation of the triangular spin-ttice in -1/2 lattice in $Na_2SrCo(PO_4)_2$. *Phys. Rev. B* **2022**, *106*, 054415.

(24) Béres, K. A.; Homonnay, Z.; Bereczki, L.; Dürvanger, Z.; Petruševski, V. M.; Farkas, A.; Kótai, L. Crystal Nanoarchitectonics and Characterization of the Octahedral Iron(III)−Nitrate Complexes with Isomer Dimethylurea Ligands. *Crystals* **2023**, *13*, 1019.